Joana Gonçalves Fernandes

Licenciatura em Engenharia de Materiais

Writing/erasing 3D micro and nano wrinkles in flexible elastomers for volatile organic compounds sensor

Dissertação para obtenção do Grau de Mestre em
Engenharia de Micro e Nanotecnologias

Orientador: Professora Doutora Maria Helena Godinho, Professora Auxiliar com Agregação, Faculdade de Ciênciase Tecnologias da Universidade Nova de Lisboa

Co-orientador: Doutora Ana Catarina Trindade, Pós-Doc do CENIMAT/I3N – Departamento de Ciência dos Materiais, Faculdade de Ciências e Tecnologias da Universidade Nova de Lisboa

Júri:

Presidente:	Prof. Doutor Rodrigo Ferrão de Paiva Martins
Arguente:	Prof. Doutor Pedro Manuel Alves Patrício da Silva
Vogais:	Prof. Doutora Maria Helena Figueiredo Godinho

FACULDADE DE CIÊNCIAS E TECNOLOGIA
UNIVERSIDADE NOVA DE LISBOA

Setembro 2014

Writing/erasing 3D micro and nano wrinkles in flexible elastomers for volatile organic compounds sensor

Acknowledgments

Gostaria de agradecer à Professora Doutora Maria Helena Godinho e à Doutora Ana Catarina Trindade pela excelente orientação e completa disponibilidade dedicada ao longo de toda esta etapa. Agradeço também a liberdade e confiança que me foi concedida durante este período, essencial para que este trabalho contribuísse, não só para o meu desenvolvimento como estudante universitária mas também, e não menos importante, para o meu desenvolvimento pessoal. Obrigada pelas horas investidas em debate e discussão de resultados, imprescindíveis para a realização deste trabalho. Não quero deixar de agradecer ao Doutor João Canejo pela sua disponibilidade ao longo de todos estes meses de trabalho.

À minha família um especial agradecimento pelas palavras de incentivo e por todo o apoio e admiração com que me brindaram ao longo destes anos, em particular um muito Obrigada aos meus Pais, Júlio e Dina, e à minha irmã Ana.

Agradeço também à família incrível que conheci em Barcelona por me mostrarem novos caminhos, cheio de novas possibilidades.

Agradeço ao Professor Doutor Rodrigo Martins e à Professora Doutora Elvira Fortunato pelo acesso às instalações e equipamentos do CENIMAT, nomeadamente nas medidas realizadas por AFM com a ajuda imprescindível do Tomás Calmeiro. É também com muito apreço que agradeço à Xana e ao Fifi por toda a ajuda na produção das máscaras.

Agradeço ainda…
Ao Alex pelos seus monólogos de grunhidos impercetíveis cheios de boa disposição;
À Pontes por me mostrar que é possível obter bons resultados apanhando gotas filtradas numa bancada cheia de poeira;
À Teresa por provar que é possível obter porosidades de 120% e pelo seu entusiasmo ao longo de milhares de horas de medições no viscosímetro.
Ao Zé Rui pela sua magia e pelo seu discurso aleatório;
Ao Trofas pela depressão eternamente sentida causada pelo episódio “O regresso do HZB”;
Ao Marreios pela péssima combinação de cores que alegra os nossos dias;
À Paula Soares e ao Francisco Ferreira pelos seus infinitos frasquinhos cor-de-rosa (nesse momento percebi que havia alguém pior).
Ao Luis Aguirre, à Coro Echeverria e à Ana Baptista, por me mostrarem que existe sempre um lado positivo, que é normalmente seguido por uma explicação científica.

Abstract

Micro/nano wrinkled patterns on cross-linked urethane/urea polymeric flexible free standing films with two soft segments, polypropylene oxide and polybutadiene, can be induced by UV-irradiation. The ability to write/erase these 3D structures, in a controlled manner, is the main focus of this work. The imprinting of the wrinkled structures was accomplished by swelling in an appropriate solvent followed by drying the membranes after the cross-linking process and UV irradiation. The surface tailoring of the elastomeric membranes was imaged by optical microscopy, scanning electronic microscopy and by atomic force microscopy. To erase the wrinkled structures the elastomers were swollen. The swelling as well as the *sol/gel* fraction and the UV radiation were tuned in order to control the wrinkles characteristics. It was found that the wrinkles wavelength, in the order of microns (1±0,25μm), was stamped by the UV radiation intensity and exposure time while the wrinkles' amplitude, in the order of nanometers (150-450 nm), was highly dependent on the swelling and *sol/gel* fraction. A prototype for volatile organic compounds detection was developed taking advantage of the unique 3D micro/nano wrinkles features.

Keywords: Micro/nano wrinkles, urethane/urea polymeric thin films, photolithography, Volatile Organic Compounds sensor.

Resumo

A impressão de micro/nano estruturas enrugadas em elastómeros flexíveis de uretano/ureia, foram obtidas através da exposição destes filmes à irradiação UV (ultravioleta). A possibilidade de escrever/apagar estas estruturas 3D, de uma forma controlada, é o principal foco deste trabalho. A impressão de estruturas enrugadas foi conseguidas por inchamento do elastómero num solvente adequado e seguido da evaporação do mesmo, que foi previamente sujeito à radiação UV onde foi promovida a formação de uma camada mais reticulada.

As estruturas formadas foram analisadas por microscopia ótica polarizada, microscopia eletrónica de varrimento e por microscopia de força atómica. O inchamento e a fração de *sol/gel*, assim como o tempo de exposição à radiação UV foram optimizados de forma a controlar as características das estruturas formadas. O comprimento de ondas das rugas, na ordem dos microns (1±0,25μm), foi definido pela radiação UV estando relacionado com a intensidade da luz assim como o tempo de exposição. A amplitude, na ordem nos nanómetros (150-450 nm), é fortemente dependente do inchamento e da fração *sol/gel*. O protótipo do sensor de compostos orgânicos voláteis foi desenvolvido tirando vantagem das propriedades das micro/nano estruturas formadas.

Palavras-chava: Micro/nano rugas, Filmes Finos de Poli(uretano/ureia), Fotolitografia, Sensor de composto orgânicos voláteis.

Abbreviations

A	Amplitude
AFM	Atomic force microscopy
DBTDL	Dibutyl tin dilaurate
f	Functionality of the polymer
LC	Liquid Crystal
(-NCO)	Isocyanate terminal functional group
(-OH)	Hydroxyl terminal functional group
PBDO	Polybutadienediol pre-polymer
PDMS	Poly(dimethyl siloxane)
POM	Polarized Optical Microscopy
PU	Poly(propylene oxide)-based triisocyanate terminated pre-polymer
SALS	Small Angle Light Scattering
SEM	Scanning Electron Microscopy
SERS	Surface Enhanced Raman Scattering
UV	Ultraviolet radiation
VOCs	Volatile Organic Compounds
W_d	Sample weight before extraction.
W_s	Sample weight immediately after extraction
W_2	Sample weight after drying
ZnO	Zinc oxide

Symbols

A	Amplitude, [nm]
E_r	Young's modulus the rigid part, [MPa]
E_f	Young's modulus the soft part, [MPa]
l	Length of swollen sample, [cm]
l_0	Length of dried sample, [cm]
t	Thickness, [μm]
wt%	Percentage by weight, [%]
λ	Wrinkles wavelength, [μm]
λ_{laser}	Laser wavelength, [nm]
λ_{UV}	Ultraviolet wavelength, [nm]
θ	Diffraction angle, [º]
υ	Shear velocity, [ms^{-1}]
ε	Strain, [%]
ε_c	Critical strain, [%]

Table of Contents

List of Figures

List of Tables

Objective

The main goal of this work was to control and manipulate tunable equilibrium micro/nano structures in flexible elastomeric poly(urethane-urea) membranes. The cross-linked urethane/urea polymeric free standing films with two soft segments, polypropylene oxide and polybutadiene, were prepared by reacting a poly(propyleneoxide)-based triisocyanate-terminated prepolymer (PU) with polybutadienediol (PBDO). Wrinkling on these elastomeric membranes is induced by UV irradiation (λ_{UV}=254nm) and permanently imprinted by swelling the membranes in a good solvent. The detailed study of the wrinkled surfaces with different *sol/gel* concentration was performed, which allowed to understand the development of the elastic instabilities in this kind of membranes (wavelength, in the order of 1μm, and amplitude in the nanoscale, from 150 to 450 nm). At the end of this work, a sensor was obtained by photolithography process, allowing micro/nano 3D writing in a flexible substrate, which is also sensible to volatile organic compounds.

Chapter 1 – Introduction

1.1. Motivation

During the last decades, the improvement of nano-microstructures in soft matter has been challenging. The fabrication of structured polymer surfaces, for a wide range of applications, from optics and flexible electronics [1] to biological cell studies[2], have been mainly developed in two distinct ways; resorting and adapting techniques as embossing [3,4] or nano-microimprinting [5] or by developing novel techniques as well soft lithography [6] or laser scanning among others.[7]

In another perspective, these patterns can be obtained by regarding the inherent properties of the polymeric materials. It is possible to produce these structures by inducing surface instabilities by different mechanisms, taking advantage of the intrinsic materials properties. In this sense, the interest on complex patterns obtained by self-organizing processes becomes a very important issue since it is difficult or makes nearly impossible its production by traditional methods.[8]

The creation of artificial micro/nano ripples arises from the interest of mimicking similar structures found in nature, example of *Drosophila melanogaster* [9]. Yet, manufacturing and controlling these structures at the nanoscale is highly challenging, even more if a fragile and flexible substrates are used. In this sense, the most explored method and the center of this work is the formation of micro/nano wrinkles in a flexible elastomer due to its surface instabilities, where the control of the wrinkles amplitude and period takes a prominent role.

1.2. Urethane/Urea Elastomers

Urethane/urea elastomers are copolymers formed by reacting monomers with isocyanate terminal functional group (-NCO) and hydroxyl (-OH). In the synthesis of polyurethane, the aliphatic prepolymers used often have functionality greater than two, which gives rise to the formation of segmented three-dimensional polymeric networks. These segmented polyurethane elastomers are composed of long flexible chains, provided by polyol, connected by rigid aromatic segments of polyurethane and polyurea. In this case, the rigid urethane segments and flexible segments of the polyol are immiscible, meaning that, although the polyurethane materials are macroscopically isotropic, they are not structurally homogeneous at the microscopic level. Even though both the hard and soft segments present a certain degree of miscibility between each other, the phenomenon of phase separation (micro-segregation) of these two segments it is inevitably. As a result, the phase-separated hard-segments will form domains (crystalline and ordered) dispersed within a soft-segment matrix.

In the synthesis of elastomers in study, two kinds of starting monomers were used, a prepolymer of polyurethane, specifically poly(propylene oxide)-based triisocyanate terminated

(PU) and a pre-polymer of polybutadienediol (PBDO).This type of material (pre-polymer) is used in the synthesis of elastomeric poly(urethane-urea), allowing their terminal functional groups to react with one another to give a cross-linked polymer (network).[13]

The prepolymers of PBDO (functionality *f* = 2) emerged from the modification of the polybutadiene by introducing two terminal hydroxyl groups. The introduction of these groups allows the use of this prepolymer in the production of new elastomeric materials by reaction with other prepolymers with different functional groups (in particular with the prepolymer of isocyanate-based urethane). The urethane prepolymer, PU, used in the synthesis of the elastomeric film under study is based on polypropylene oxide and has three isocyanate reactive end groups (functionality *f* = 3).

The synthesis and preparation of urethane/urea elastomers with two soft segments, polypropylene oxide and polybutadiene, have been reported[14] and were mainly studied in order to prepare pervaporation membranes with improved permeation performance. In an earlier study, it was shown that flat urethane/urea segmented elastomer films can exhibit distinct functionalities, that occur on one of its surface resulting from the surface textures generated by the ultraviolet (UV) irradiation and upon the application of a mechanical field and/or solvent extraction [13]. The control of the periodicity of such structures is in fact an essential parameter, and is already known that the UV irradiation time is the main important condition for the formation of the wrinkles, with a well-defined wavelength. [15]

1.3. Surface wrinkling

If we look into nature, wrinkles appear when a mechanical force is applied on skin, for example, muscle contraction or mechanical compression. Regarding to the particular case of skin, it is formed by a thin layer of the epidermis, relatively rigid, which is joined to a layer which is about ten times thinner, which is much more flexible (the dermis). As we get older, the dermis (less rigid layer) contracts, leading the system into a compressive stress, appearing skin wrinkles in response to this tension. [8]

However, according to Genzer and Groenewold[16], nature gives us plenty examples that are ruled by this phenomenon. This said, wrinkled surfaces not only appear in human or fruit skin by stretching/compression, as these same principles may be applied to the formation of mountains due to the compressive tectonic forces. Hence, the wavelength of these wrinkling surfaces may range from kilometers, down to the nanometer size: which is the case of polymeric materials surface such as poly (dimethyl siloxane) (PDMS), studied by Efimenko [17] where wrinkled surfaces were obtained by exposure to ultraviolet (UV) radiation and stretching.

Concerning this topic, the first study on pattern formation of similar structures was reported by Tanaka group[19], which was then followed by numerous and different theoretical and experimental theories[18] to understand the formation mechanism. Burrel *et al.* were the firsts to notice the role played by the formation of a rigid layer in the substrate and its influence in the development of the wrinkled surface.[20] Nowadays, it generally admitted that wrinkles appear as a consequence of an applied force, such as heating, mechanical stretching/compression or by drying from a swollen state (which induces a stress above a critical value). [21,22]

The creation of this rigid layer on the surface may be achieved from several different ways. Yet, one will exclusively focus for the case where this rigid layer is formed by UV irradiation. The mechanism of wrinkle formation is due to the cross-linked gradient that occurs in the film during the exposure to UV light, consequently the top layers will behaves as a rigid skin, firstly reported by Basu *et al.* [23]. The effect of UV at the molecular level was already investigated by Godinho and Trindade *et al.*[24,25] For this particular elastomers in study (PU/PBDO), it was evidenced that UV irradiation promotes new crosslinks in the exposed surface, that allows the formation of the rigid layer and consequently, after an applied force, the production of the wrinkled pattern. In the swelling method, as a way to induce the formation of the winkled pattern, the soft layers of the polymeric material induce a compressive strain on the rigid layer during the drying, and when this strain is higher/equal than the critical strain (ε_c) the wrinkles will appear. [8]

Thus, another key parameter is the amount of stress or strain needed to induce wrinkling in the system. A mathematical study of these instabilities was applied to laminates in the form of sandwich panels, the simplest of which is comprised of two relatively thin, stiff sheets of materials bonded to either surface of a thick, compliant material. Upon compressive loading, a buckling-type instability can occur on the surface of the laminate, where the surface begins to wrinkle with a defined wavelength (λ) and amplitude (A). In this case, it was derived that the critical strain can be determined through equation 1[26]:

$$\varepsilon_c = \frac{1}{4}\left(\frac{3 \times E_r}{E_s}\right)^{\frac{2}{3}} \qquad Eq.1$$

This parameter only depends on the ratio of the Young's moduli of the rigid (E_r) and the soft (E_f) part, and it is not affected by the thickness of the film.[26]

The amplitude and the wavelength of the wrinkles are other two important parameters to characterize the wrinkled surface. The wavelength is dependent on the thickness of the rigid layer (t) and on the ratio of the Young moduli, defined in equation 2:[17]

$$\lambda \propto t\left(\frac{E_s}{3 \times E_r}\right)^{\frac{1}{3}} \qquad Eq.2$$

The amplitude can be obtained from the strain (ε) and the critical strain, defined by equation 3: [26]

$$A \propto \sqrt{\frac{\varepsilon - \varepsilon_c}{\varepsilon_c}} \qquad Eq.3$$

This equation is the basis of the surface wrinkling metrology. These three main parameters, ε_c, λ and A, capture the central aspects of surface wrinkling: the strain at which the wrinkling instability occurs; the wavelength of the instability; and the amplitude growth as a function of strain.

1.3.1.Applications

The possibility to control the wavelength and amplitude of the wrinkles induced on the soft matter surfaces, results in a wide range of applications.[27]

Recently, wrinkled surfaces were used as a template to produce surface arrays. Schweikart *et al.* [28] confined a nanoparticles suspension between the glass substrate and the wrinkled surface, resulting in an alignment of the nanoparticles after drying and removal of the wrinkled surface. The surface enhanced Raman scattering (SERS) is a technique which allows for ultrasensitive detection of molecules but requires a well prepared substrate, able to provide a reproducible SERS signal. The possibility to create ordered arrays of nanoparticles can be applied to develop substrates for SERS, such the one of an organized array made of gold nanoparticles [28,29]

In the field of electronics, materials with bend and stretch abilities hold the promise of the new generation of flexible substrates. A recent example of the applicability of wrinkled surface was reported by Wu *et al.*[30], in this research they used a PDMS wrinkled substrate in the design of stretchable organic thin film transistors able to work on compressive and stress conditions, due the possibility from the substrate to change its amplitude and wavelength during the mechanical testing. The PDMS was also used by Kim and coworkers [31] with a UV treatment, which the swelling in ethanol induces a variation in its optical properties, from transparent to translucent. This fact is explained due the interaction between the wrinkles and the light: the ethanol induces the formation of wrinkles on the surface, resulting in a higher light scattering comparison with the dry state case, where the wrinkles disappear, causing a smooth surface and consequently becoming transparent.

In another approach, Ohzono *et al.* [32] reported the alignment of a nematic liquid crystal (LC) induced by the microwrinkles template. Basically, it was demonstrated that the possibility of changing configuration of the wrinkled surface, by strain, lead to an induction on the reorientation of the liquid crystal, which is required for the appropriate operation of LC devices.

1.4. Volatile Organic Compounds Sensor

Nowadays, the detection of volatile organic compounds (VOCs) has attracted much attention, as the inhalation or contact with these materials, such as toluene, acetone, ethanol, acetaldehyde, is indeed a health concern. Toluene, per example, is a benzonoid aromatic hydrocarbon and is known to be neurotoxic VOC. This specific compound is emitted during the production of fuels from crude oil, being used in the production of paints, adhesives and rubber.[33]

There are some traditional methods for the VOCs detection, such as the gas chromatography that is a sensitive method which can detect toluene vapors. However, the tools size and consequently the involved cost becomes a disadvantage. The increased concern about environmental protection has led to continuous search for new volatile organic compounds sensor materials, such as conductive type sensors based on metal oxides [34–36]

The toluene detection is also important in liquid state and a recent study by Partridge *et al.*, has developed a sensor based on optical fiber, with a functional nanostructured coating of calixarene, which can detect toluene contamination in water. The developing of this sensor leads to a sensing ~100 ppm concentrations of toluene.[36]

In other approach[37], the n-type semiconductor zinc oxide (ZnO) has been used as a sensing material in a metal-oxide-semiconductor devices structure for the VOCs detection. In particular, ZnO nanowires have the ability to induce a rapidly and effectively gases diffusion through the devices and consequently more atoms can participate in the surface reaction, leading to a high gas sensing performances. In order to improve it, the ZnO nanowires were functionalized with gold nanoparticles, using nontoxic and cost-effective method, and the speed response, sensitivity and selectivity in benzene and toluene detection is greater in comparison with the original ZnO NW sensor. Besides, the stability of the sensor indicates its great potential for practical application and after five months the sensing was still about 1 ppm.

In the field of transparent and flexible electronics, a toluene sensor was also fabricated by Choi *et al.* [33] based on standard microfabrication process on silicon oxide/ silicon and poly(ethylene terephthalate) substrate. Graphene was used as sensing material and led to a sensing of 10 ppm of gashouse toluene molecules at room temperature, maintaining optical transmittance and mechanical flexible properties.

Chapter 2 – Experimental and Characterization Techniques

Elastomeric thin flat films were prepared according to the procedure described earlier in the literature[14] , from a precursor solution composed of a poly(propylene oxide)-based triisocyanate terminated prepolymer and hydroxyl-terminated polybutadiene, using a selective catalyst, dibutyl tin dilaurate (DBTDL), dissolved in toluene.

PU was purchased from a Portuguese petrochemical industry (CPB) with a molecular weight of 3500 g mol^{-1}, and PBDO was purchased from Sigma-Aldrich and consists of a mixture of cis and trans isomers, with a number-average molecular weight of 2800 g mol^{-1}. Both prepolymers were dissolved in toluene and one drop of the catalyst (DBTDL) was added in order to promote the reaction between the cyanate end groups of PU and the hydroxyl end groups of PBDO, under nitrogen at room temperature (see Figure 2.1). The solid content is about 40 wt% (i.e., about 60 wt% of toluene) and the ratio of PU and PBDO was 60PU/40PBDO (wt%). An idealized chemical structure of the elastomer under study appears in reference. [25]

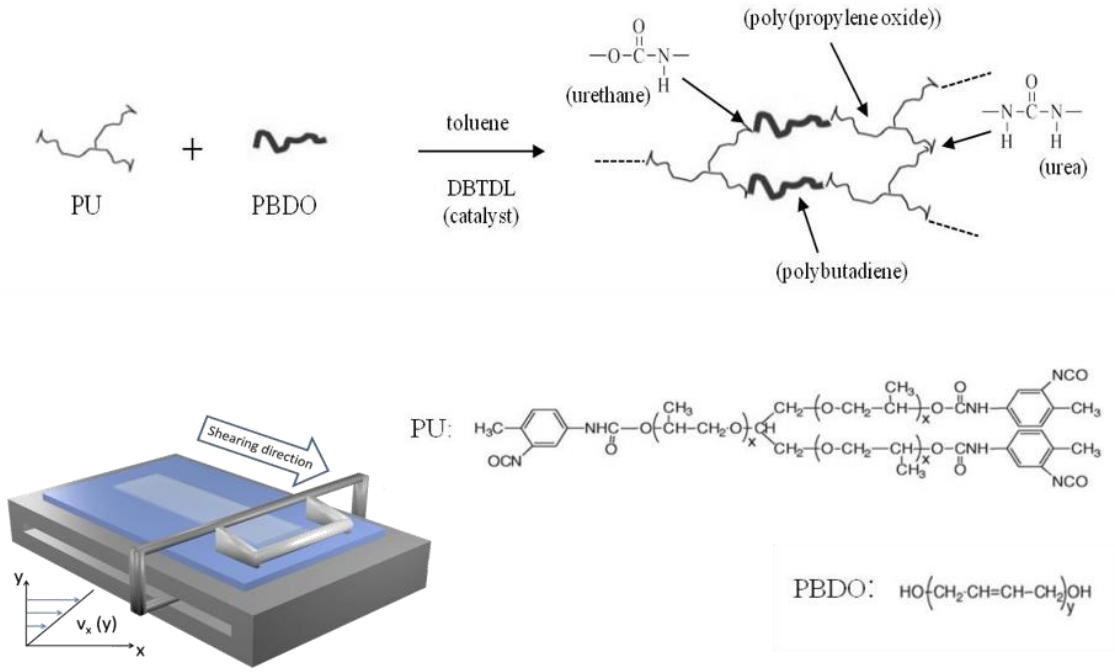

Figure 2.1 - Preparation of poly(propylene oxide) (PU)/polybutadienediol (PBDO) bi-soft segment urethane/urea elastomers (PU, x=20; PBDO, y=50). The two prepolymers were first dissolved in toluene, with one drop of catalyst. The reaction was allowed to proceed during 30 minutes and the viscous solution obtained was cast onto a treated glass (solution of 20 wt% of silane in ethanol) and sheared by moving a casting knife at a controlled shear velocity (υ =5mms^{-1}). The free-standing solid elastomer film is then removed from the treated glass substrate after curing (72h) in atmospheric moisture. The molar ratio of PU/PBDO used can be varied in order to achieve different chemical and physical characteristics. In this work it was studied a 60PU/40PBDO (%wt) ratio.

After 30 min reaction (and before gel point), the precursor solution was cast onto a treated glass plate (solution of 20 wt% of silane in ethanol) and sheared, at room temperature, with a calibrated Gardner knife moving with a controlled rate, υ = 5 mm s^{-1}. The elastomeric film was removed from the glass substrate after cured in an oven at 70–80 ºC for 3 h followed by cure in air during 3 days. The final thickness of the films was measured using a Mitutoyo digital micrometer (about 100 µm).

The top surface of the PU/PBDO thin flat film was UV-irradiated (λ_{UV} = 254nm) for 24h, and a wrinkling pattern surface appeared after *Soxhlet* extraction in toluene, varied from 3h30, 9h, 16h, 24h and 27h, at 60 ºC and drying.

Polarized optical microscopy (POM) was used for the morphology of the wrinkling surface, specifically for the wavelength measuring, and was confirmed by scanning electron microscopy (SEM) using a SEM DSM962 model from Zeiss. Gold was deposited on the film by sputtering in an Ar atmosphere, using a 20 mA current, for 30 seconds at a deposition rate of 3 A s^{-1}. SEM images were captured at an acceleration voltage of 5 kV. Small angle light scattering (SALS) patterns was obtained with a red (λ_{laser}=633 nm) helium neon laser equipped optical bench, for the samples which were extracted in toluene during 24 hours, with the help of a CCD video camera.

Atomic force microscopy (AFM) was used to characterize quantitatively the topographical features of the films, mostly for the amplitude, after 24 hours in UV-radiation and after *Soxhlet* extraction with toluene for all samples. The AFM measurements, carried out in alternate contact mode under ambient conditions, were obtained by using a commercial Olympus AC160TS (silicon) with spring constant of 42 N/m and oscillation frequency of 300 KHz. The scanned area was 20 µm x 20 µm and 5 µm x 5 µm, and the scan rate was 0,7 Hz and 1Hz respectively.

The variation of transmission intensity was measured during the toluene evaporation for all samples with the red (λ_{laser}=633 nm) helium neon laser equipped optical bench. The sensor response to different solvent, such as toluene, acetone, ethanol and water, was also measured by the same technique. This sensor was produced by photolithography, where the sensing letters were written with wrinkles using the same procedure as the sample for the 27h, meaning 24h expose to UV radiation and 27h in toluene extraction.

Chapter 3 – Results and Discussion

3.1. Swelling and sol-gel extraction

The crosslinking reaction leads to the formation of two distinctive parts within the material: the gelled part, known as *gel*, which is insoluble; and the *sol* which, in contrast to the previous one, is soluble. Therefore, quantifying both the gel and sol fraction is possible by extracting the sol with a specific solvent. This method is commonly known as *sol-gel* extraction method. Previous studies[38] have shown that toluene (ie, the solvent in which the reaction PU-PBDO is carried on) is an appropriate solvent to be used in this method as it provides a greater swelling degree of the elastomeric samples, so it was chosen as the solvent for this particular case. In this experimental work, the maximum swelling of the 60PU/40PBDO samples was around 340±16% wt%. The following expressions are related to the swelling percentage (equation 4), the percentage of gel (equation 5) and extracted sol (equation 6):

$$\%\, swelling = \frac{W_s - W_2}{W_2} \times 100 \qquad Eq.4$$

$$\%\ \ gel = \frac{W_2}{W_d} \times 100 \qquad Eq.5$$

$$\%sol = 100\% - \%\, gel \qquad Eq.6$$

Where W_s is the sample weight immediately after extraction,W_2 is the sample weight after drying in a oven and W_d is the sample weight before extraction.

The evolution of *sol-gel* extraction process was followed in time, from 3h30minutes to 27h (Figure 3.1). When the elastomeric free-standing film is swollen in toluene, both inner and outer stiffer shell deform by the same amount and the *sol* composition in the film varies, depending on the time of the *Soxhlet* extraction. After 3,5h and as the swelling time increases, it is possible to observe a decreasing of the *sol* fraction (*i.e.*, unreacted polymer blocks) in the elastomeric film. The mechanism that seems to rule this process is the diffusion out of the swollen *sol* into the surrounding solvent bath.

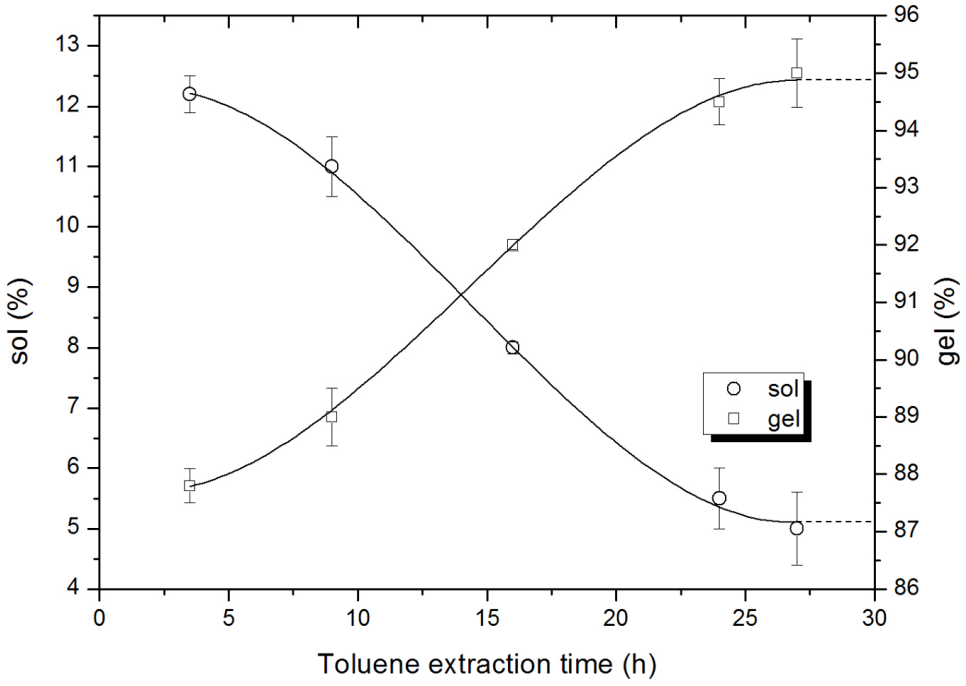

Figure 3.1 - Evolution of the *sol* and *gel* fractions vs of time. The dashed lines are just a guide for the eyes.

3.2. Wavelength

This experimental work aims to investigate the influence of the toluene extraction time (and, consequently, the % of sol extraction) on the final wrinkled patterns obtained in 60PU/40PBDO elastomeric free-standing films. The wrinkles were obtained by swelling in an appropriate solvent (toluene) followed by drying the 60PU/40PBDO elastomer that was prior exposed to the UV radiation for 24h. In this work it is presented experimental observations of wrinkled morphologies, controlled by changing the swelling time in the *Soxhlet* apparatus (which was varied from 0 to 27h). Figure 3.2 shows polarized optical microscopy (POM) images, taken in transmission mode and between parallel polarizers, for different extraction times of the films in toluene: 0h, 3h30, 9h, 16h, 24h and 27h.

From the POM images shown in Figure 3.2, it is possible to observe that initially (after UV irradiation and before *Soxhlet* extraction) the surface of the elastomer remains smooth, but once the extraction time increases the UV irradiated surface shows a corrugated pattern, with features of μm-sized in all axes, resulting in a dramatic increase in the roughness.

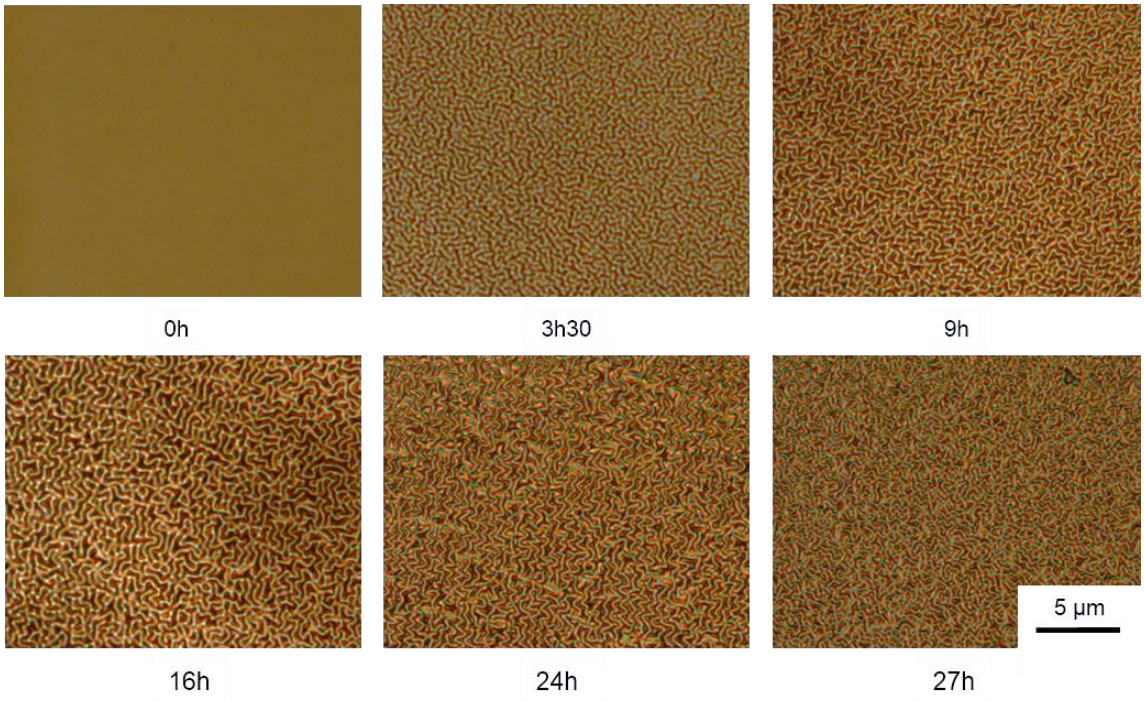

Figure 3.2 - Polarized optical microscopy (POM) images of a 60PU/40PBDO sample after being exposed to UV radiation during 24h and extracted in toluene for different periods of time: 0h, 3h30, 9h, 16h, 24h and 27h.

As already explained in chapter 1.3, these materials can be characterized by the distance between two consecutive “bands” (or peaks) – “wavelength”. SEM imaging enables this quantification through surface topography examination of the elastomeric films, as shown in Figure 3.3.

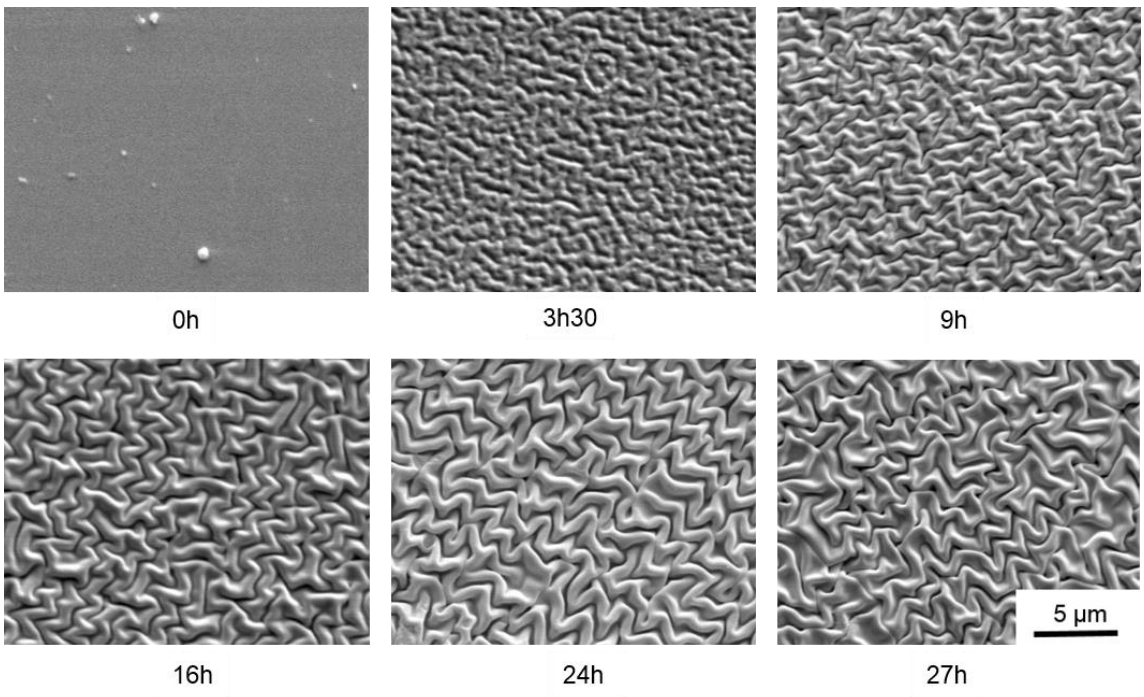

Figure 3.3 - SEM images of a 60PU/40PBDO sample after being exposed to UV radiation during 24h for different periods of extraction time: 0h, 3h30, 9h, 16h, 24h and 27h. These images confirm the observations obtained by POM.

SALS patterns were obtained using the procedure described earlier (chapter 2), allowing the determination of the characteristic periodicity distance, which can be compared with the results obtained from POM and SEM pictures. Figure 3.4 (b) shows a top view topography image of the SALS pattern obtained for the film UV-irradiated and extracted in toluene during 24 hours.

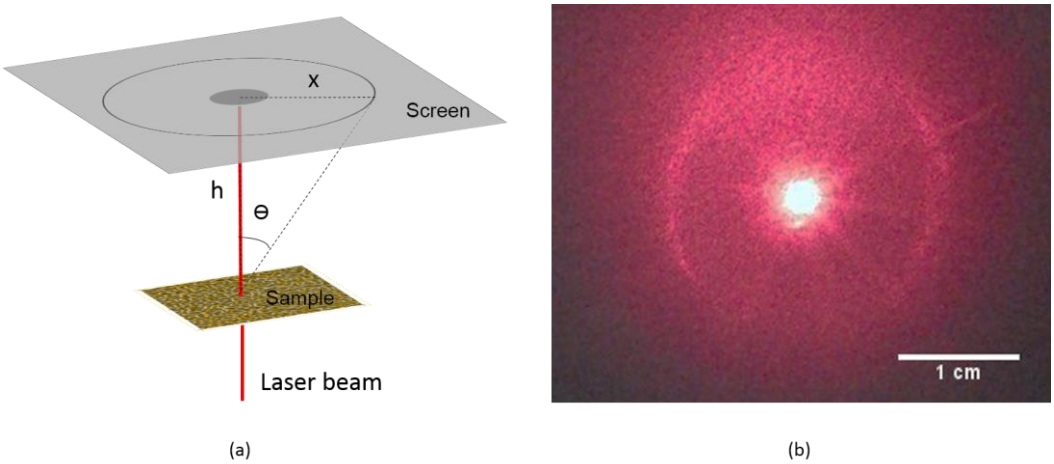

Figure 3.4 - (a) Schematics of the SALS technique measurements, where the distance between the sample and the screen is h = 4,20cm; and the distance between the laser spot and the scattered image is x = 1,21cm. (b) Light scattering pattern developed for a 60PU/40PBDO film after UV exposure for 24h *Soxhlet* extraction time.

The wavelength of the wrinkles presented in the elastomeric surface pattern can be obtained from the SALS pattern by resorting to the Bragg law ($n\,\lambda_{laser} = 2\,\lambda \sin\Theta$), knowing the wavelength of the laser used, λ_{laser}= 633 nm, and the diffraction angle, θ (obtained from the relation between the distance between the sample and the screen, h = 4,20cm, and the distance between the laser spot and the scattered image, x=1,21cm). For the given pattern (Figure 3.4 b, 60PU/40PBDO) it is possible to obtain the wavelength of the wrinkles presented in the elastomeric surface pattern: λ = 1,15μm. This value is in agreement with the ones obtained by analysis of the correspondent microscopic, SEM and POM, images: λ = 1,0±0,25μm.

The same procedure was made for the 60PU/40PBDO samples extracted for different periods of time (from 3,5h to 27h). The results obtained for all the samples with the three different methods (POM, SEM and SALS) are in accordance with each other and there are no significant wavelength variations in the wrinkled pattern observed for the different extraction times in toluene. These observations seem to indicate that it is the time of UV exposition which determines the wavelength of the wrinkles in the elastomeric film surface, as it is independent on the time of *Soxhlet* extraction in toluene.

3.3. Amplitude in function of toluene extraction time

The amplitude of the wrinkles (*ie*, peak to valley distance) obtained in the elastomeric free-standing film surface can be determined by AFM topographic images. These images (20x20 μm^2 area scanning) were obtained for different times extraction in toluene, from 3h30 to 27h and are shown in Figure 3.5.

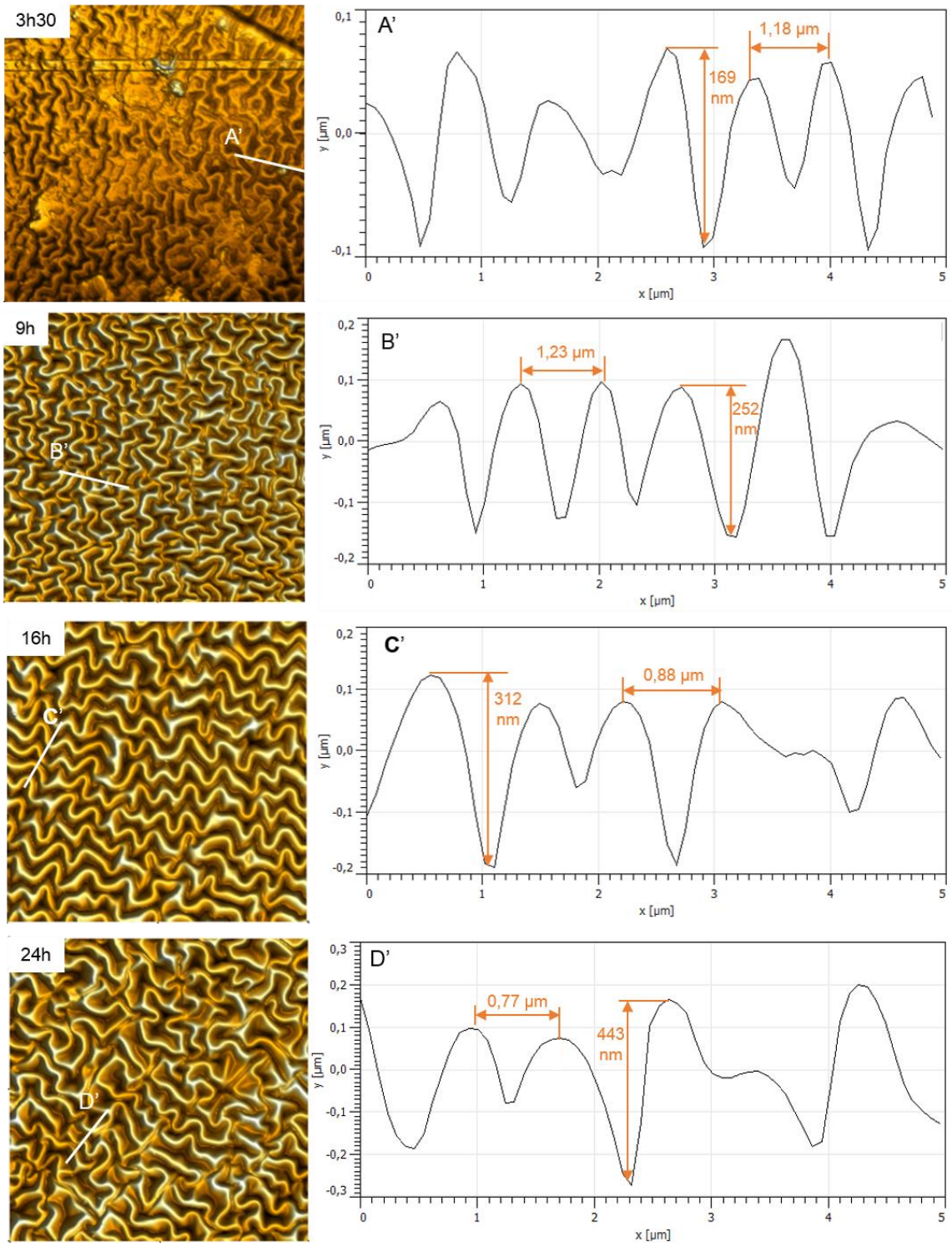

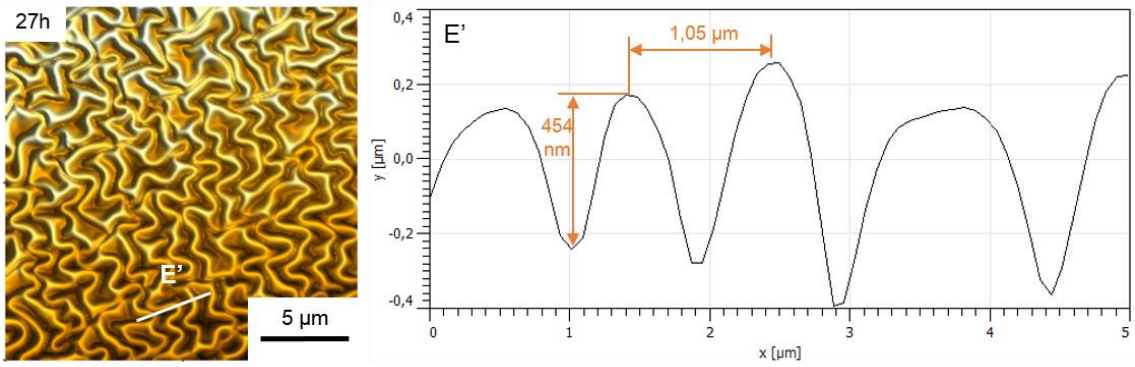

Figure 3.5 - AFM topography images of a 60PU/40PBDO sample after being exposed to UV radiation during 24h for different periods of extraction time: 3h30, 9h, 16h, 24h and 27h; the A' to E' cross-sections were taken along the lines marked on the 2D images.

The corresponding 3D AFM images for a 5x5 μm^2 area scan are shown in Figure 3.6.

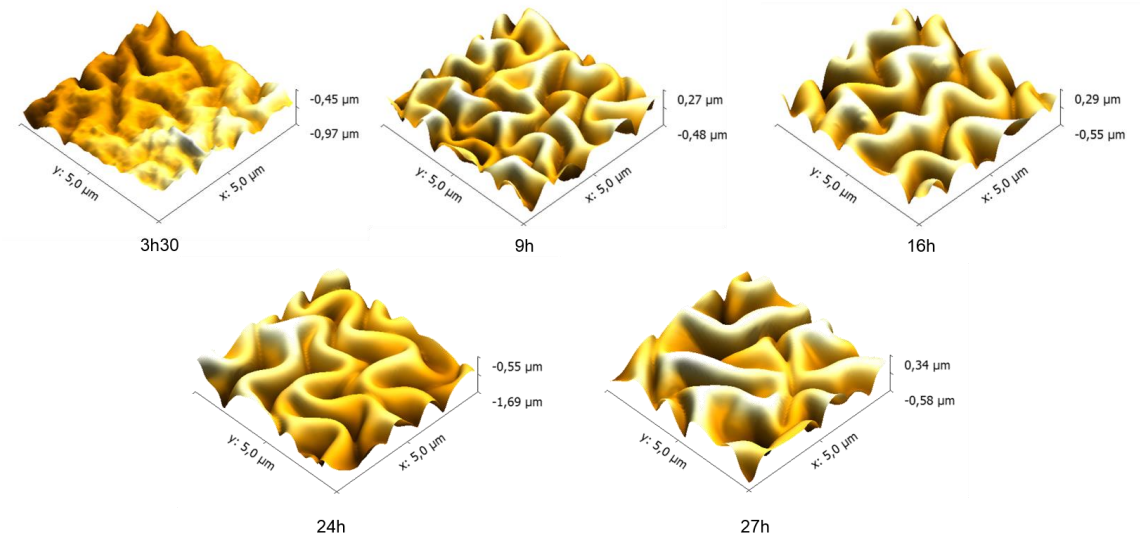

Figure 3.6 - AFM 3D images of a 60PU/40PBDO sample after being exposed to UV radiation during 24h for different periods of toluene extraction time: 3h30, 9h, 16h, 24h and 27h.

AFM analysis enables the determination of the amplitude of the wrinkles and the average roughness (Table 3.1) at the UV-irradiated surface of the free-standing elastomeric film. By more, by using the topographic images, it is also possible to determine the already measured wavelength data and confirm the results obtained via POM, SEM and SALS.

From table 3.1 it is possible to observe an increase in the amplitude data from 168 nm to 421 nm, corresponding to 3h30 and 27h, respectively. This increase is more evident between 3h30 and 16h, which corresponds to the biggest variation in the sol extraction (Figure 3.1), which is an indication that it is not only the swelling of the elastomer the responsible of the roughness in the surface of the elastomer but also the extraction sol fraction (and consequently the increase of the % of gel in the material). Therefore it is possible to relate the amplitude of the wrinkles at the surface of the film with the percentage of sol extracted: the higher the sol fraction extracted, the greater the amplitude of the wrinkles.

Table 3.1 - Evolution of the average roughness and amplitude of the wrinkles observed in the UV-irradiated elastomeric PU/PBDO for different extraction times in toluene

Toluene extraction time (h)	Average roughness (nm)	Amplitude (nm)
3,5	78	168
9,0	111	280
16,0	145	343
24,0	158	412
27,0	173	421

Figure 3.7 shows the behavior of the amplitude of the wrinkles appeared at the surface in function of % of sol that remains in the elastomer and its wavelength, which is constant.

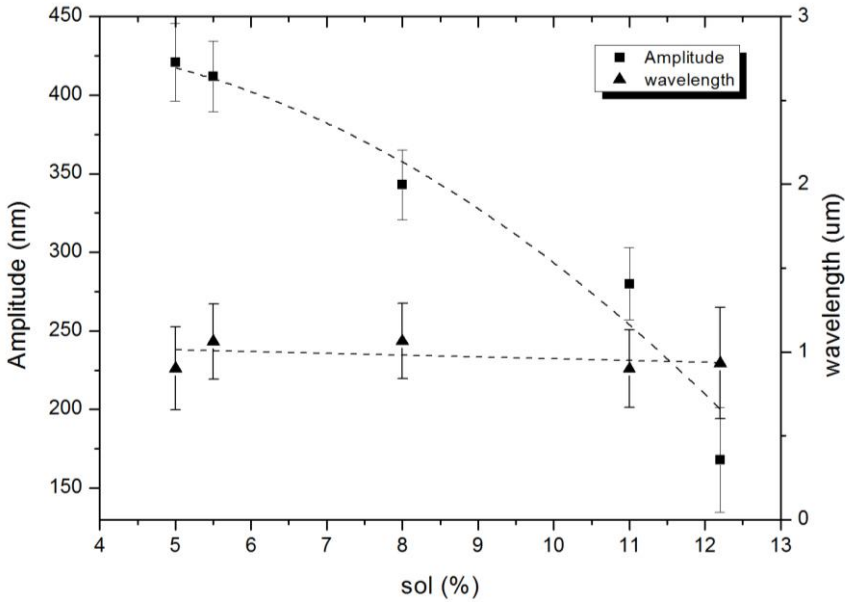

Figure 3.7 - Evolution of the amplitude of the wrinkles that appeared at the surface of the elastomeric 60PU/40PBDO free-standing film after UV-irradiation in function of the % of sol fraction that remains in the elastomeric film. The dashed lines are just a guide for the eyes. The amplitude of the wrinkles increases with the increasing % of sol extracted from the film (and with the increasing of the extraction time in toluene). The corresponding wavelength of the wrinkles is also plotted and it remains constant in time, $\boldsymbol{\lambda \approx 1\mu m}$.

As mentioned in chapter 1.3., the wrinkled surface at the urethane/urea elastomer in study appears after swelling and unswelling the elastomeric film in an appropriate solvent, and, so, the nature of these wrinkles are not the same as one the proposed and gave rise to equation 1. Although, this equation can give a rough estimate for the critical stress needed to induce wrinkles in the 60PU/40PBDO system: ε_c = 42% (E_f/E_s= 1,4 for the 60PU/40PBDO system). Experimentally it is possible to determine the amount of stress applied to the sample during the different extraction times in study. This amount is calculated from the length dimension of each sample, measured immediately after extraction (swollen sample, l) and the dried one (l_0), $\varepsilon = (l-l_0)/l_0$. According to the measures obtained, the stress induced for all the samples extracted

between 3,5h and 27h was the same, about 64%. This is an indication that all the samples were studied for their maximum swelling and the only change in this sample is % of sol within the material.

3.4. Influence of wrinkling surfaces in light transmission intensity

The results on the influence of toluene extraction time in the final wrinkles morphology developed an interest towards the influence of these different structures in the light scattering. Figure 3.8 represents the variation of the light transmission intensity during toluene evaporation for the five different extraction times in toluene in study. In this measurements, films response time have not been taken into account as it was observed that there is a direct relation between the sample´s size and its inherent response time which was not possible to control. Consequently and for a better and more intuitive analysis, all plots were set at 3 min, however this exact time has no physical meaning. The plots presented in Figure 3.8 are the average data for five measurements for each swollen/extracted sample.

Analyzing Figure 3.8, it is possible to observe that both 0h and 3,5h extraction in toluene times did not promote any variation in the transmission intensity, thus having 100% of transmitted light – the 60PU/40PBDO UV-irradiated films remain transparent. Increasing the extraction time, it can be observed variations between the light transmission intensity initial and final values. The plotted data for the samples extracted from 9h to 27h shown a similar behavior.

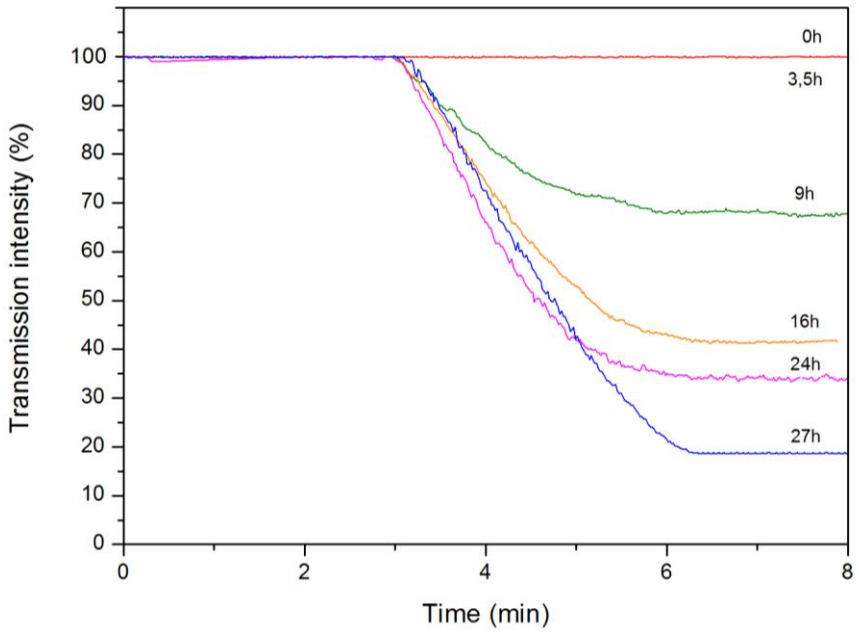

Figure 3.8 - Variation of the light transmission intensity of the swollen 60PU/40PBDO UV-irradiated elastomeric film during toluene evaporation for different toluene extraction times. It can be clearly observed that the final stage of the elastomeric sample changes from transparent (swollen) to translucent stage (dry) and that the extraction in toluene time increases the opacity of the sample.

In addition, it is possible to conclude that the extraction in toluene time increases the opacity of the sample, *i.e*, more time of extraction with toluene in the *Soxhlet* apparatus (less % of *sol* in the sample), less transparent is the dried elastomer. This is in agreement with the observations obtained from the microscopic images (POM, SEM and AFM) related with the increase of the amplitude in the elastomeric UV-irradiated surface.

In Figure 3.9 are represented the final transmission intensities of the five studied samples and the average amplitude of the wrinkles at the elastomeric surface measured previously (Paragraph 3.3). Comparing all the results, it is possible to observe a relation between the sample amplitude and its final transmission intensity, where a higher amplitude of the wrinkles directly affects the transmitted intensity to lower values and a more translucent sample is achieved. This observation is due to the fact that the extraction time of the sample in toluene increases the extraction of the *sol* portion within the sample, and increases its average roughness surface, which makes the film less transparent.

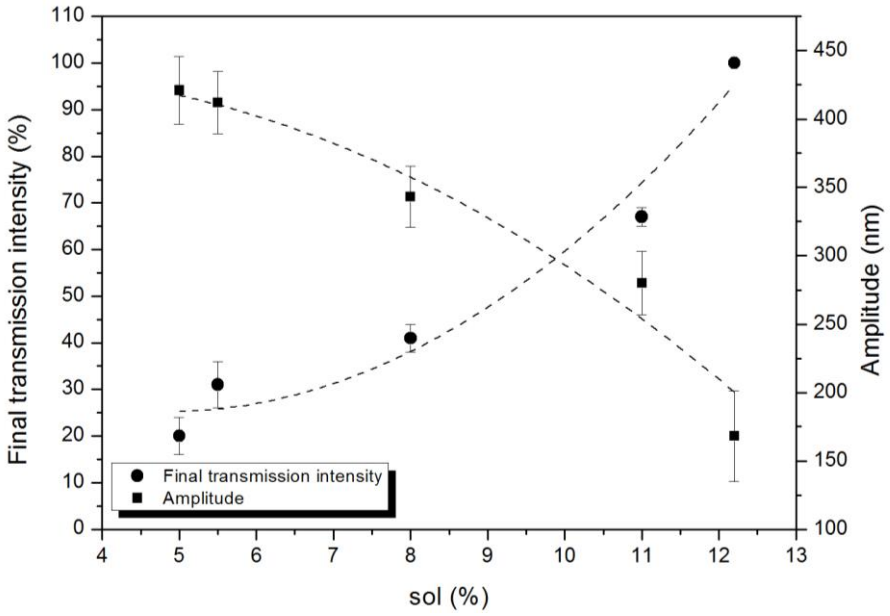

Figure 2.9 - Final transmission intensities of the five studied samples and the average amplitude of the wrinkles at the elastomeric surface. The dashed lines are just a guide for the eyes. As the amplitude of the wrinkles at the surface of the film (and, consequently, the average roughness of the surface) increases, the dried elastomeric sample becomes more translucent and less transparent.

In order to confirm the role of the extraction of the *sol* fraction in the elastomeric network, all these samples were submitted to a second extraction in toluene. They were allowed to dry and the final light transmission intensity was measured. For all the samples it was obtained the same value (about 20%), which is an indication that the variation in the amplitude (and the average roughness) of the wrinkled surface in these PU/PBDO elastomers is mainly related to the *sol* extraction during the *Soxhlet* procedure.

3.6. Volatile Organic Compounds Sensor

Taking advantage of the existing relation between the wrinkled pattern and the scattered light, this material may be further developed into a solvent sensor. Godinho *et al.* have already done photolithography in these substrates.[39] In this work, some preliminary essays were performed in order to improve the accuracy achieved in these patterns.

Figure 3.10 (a) shows a schematic of the lithographic process, where the 'FCT/UNL' pattern appears written with wrinkles. Firstly, a mask with the logo (FCT/UNL) was placed between the elastomeric 60PU/40PBDO film and the UV light. The film was irradiated (λ_{UV}=254 nm) for 24h and the desired logo was impressed in the elastomeric surface. This pattern is only observable after toluene extraction of the film, followed by drying. In Figure 3.10 (b) it is shown macro and micro-optical photographs of a toluene sensor produced during this work. In the two higher magnifications (b2 and b3) is possible to observe in detail the wrinkles that appeared written in the sensor.

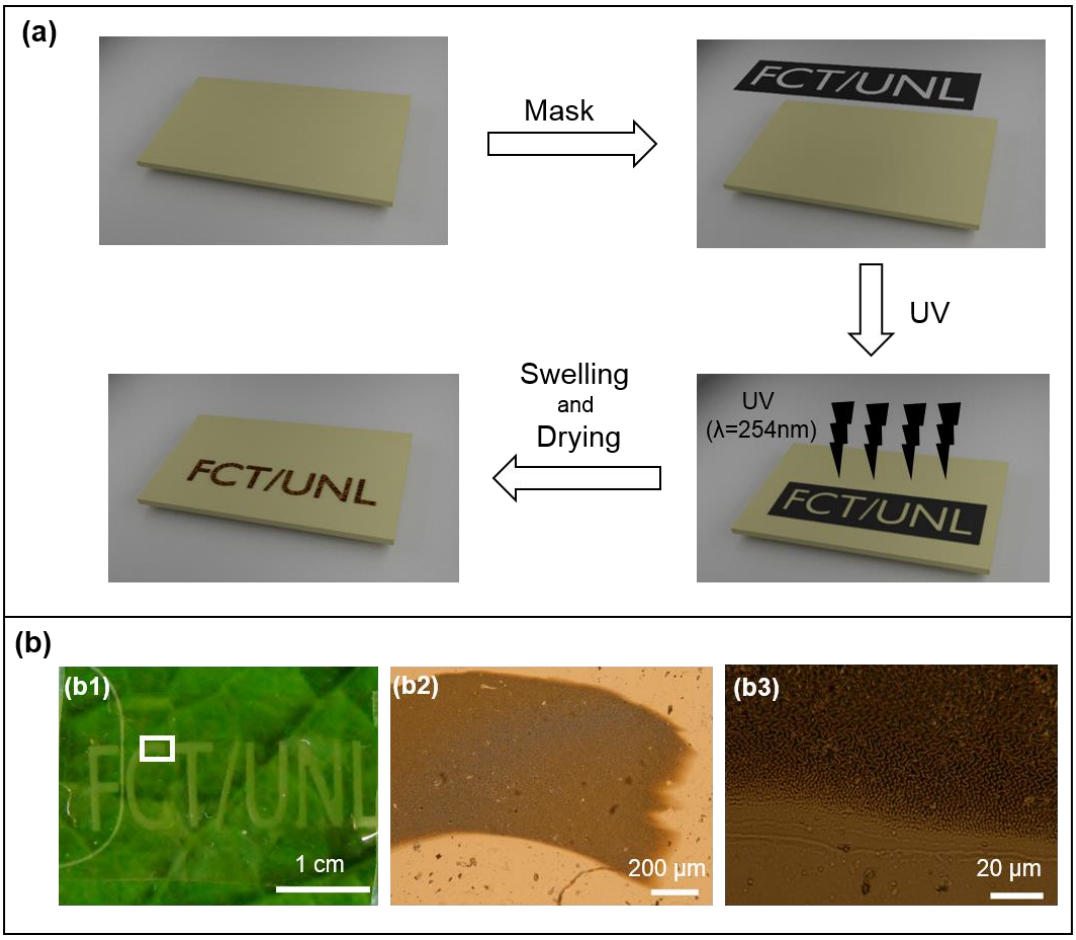

Figure 3.10 – (a) Schematics of the toluene sensor fabrication method, by a lithographic process. A mask with the pattern to imprint in the sensor is placed in the top of the elastomeric film before UV-irradiating it. Removing the mask and after extracting the film in an appropriate solvent and drying it, the chosen pattern appears written in μm-sized wrinkles. (b) Macro- and micro-optical photographies obtained for an example of a toluene sensor produced from a 60PU/40PBDO film: (b1) The letters "FCT/UNL" were written with wrinkles by UV irradiation; (b2) POM image obtained for a zoom in the limited square; (b3) higher magnification shows a detail of the wrinkles.

The observation that the films submitted to a 27h in toluene process were more translucent (20% of transmission intensity). Therefore, this extraction time is an optimization for sensing properties, meaning a highest contract between the sensing letters and the smooth surface.

Figure 3.11 shows the response of the PU/PBDO elastomeric sensor prepared through the procedure described earlier (Figure 3.10), to toluene solvent. The response of the elastomeric thin film to a toluene droplet occurs immediately: the droplet of toluene promotes the swelling of the film and, consequently, the wrinkled surface change into a flat surface, resulting in the decreasing of the translucence of the film (in a few seconds, at the maximum swelling of toluene, the film becomes transparent). In addition, the recovery time depends upon the quantity of solvent: the larger the amount of solvent, the longer the recovery time.

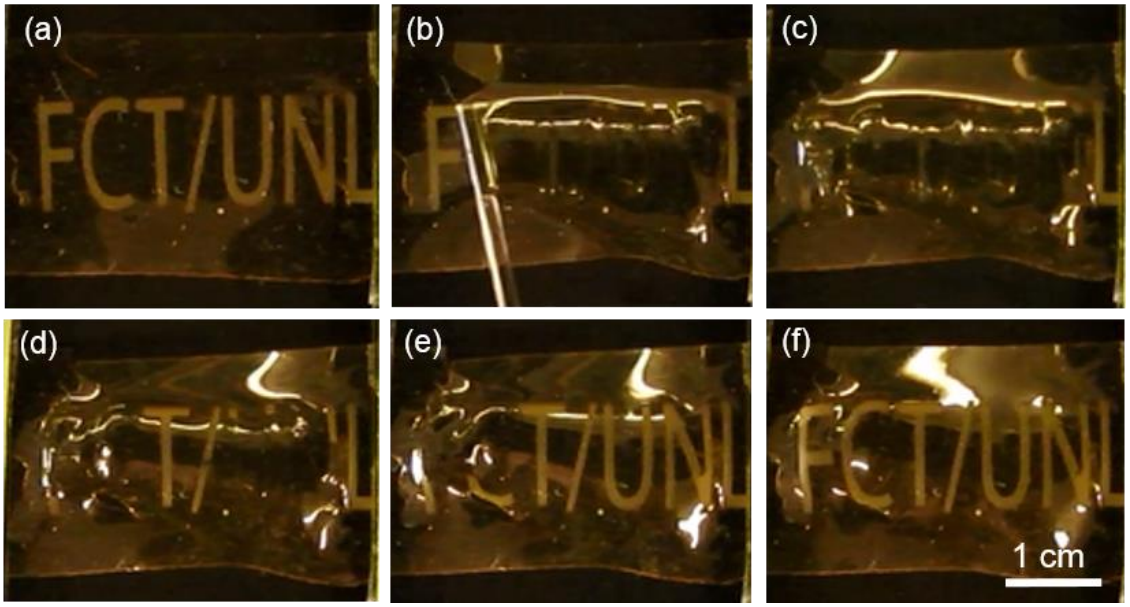

Figure 3.11 - 60PU/40PBDO free-standing film sensor response to a droplet of toluene at its surface. (a) This sensor was prepared through the procedure described earlier, and the logo “FCT/UNL” is written in the top surface. (b) After dripping a drop of toluene over the surface of the elastomeric film sensor, it is possible to observe in (c) that the wrinkled pattern is immediately erased, and the film becomes transparent. The recovery of the logo pattern is promoted by the de-swelling of the film as the solvent evaporates after: (d) 8 s; (e) 10 s; and (f) 38 s – final stage corresponding to the evaporation of all solvent and the consequent reappearance of the logo pattern.

The experimental setup of the sensor response to the dripping of a solvent droplet at the top of its surface, presented above, was also characterized by measuring the variation of transmission intensity during the toluene evaporation for the all samples. The results are shown in Figure 3.12, for four distinct solvents: toluene, ethanol, acetone and water. This solvents were chosen based on the behavior of the films to this particular solvents, where it was found that the swelling (in weight) of the60PU/40PBDO elastomeric film in toluene 340%, in acetone is 40%, in ethanol is 50% and in water is 0%.

Comparing the responses obtained for all the solvents tested with this sensor, the one obtained for toluene is the fastest times response regarding the response of the others solvents.

The most similar response is for ethanol, with a 100% of transmission intensity, yet for a much higher response time in comparison with toluene. The transmission intensity of the acetone is about 92%, meaning the swelling was not enough to promote a complete smooth surface. The lowest response time is observed for the water case, where the impregnation of the solvent into the film takes roughly 26 min for a poor transmission intensity of 86%. In Figure 3.12 it is also observed that for the four solvents in study, the PU/PBDO sensor completely recovered its initial transmission intensity, 20%. The acetone promoted an unusual behavior comparison with the other responses, the transmission intensity falls to 10% and them stabilizes for the 20%

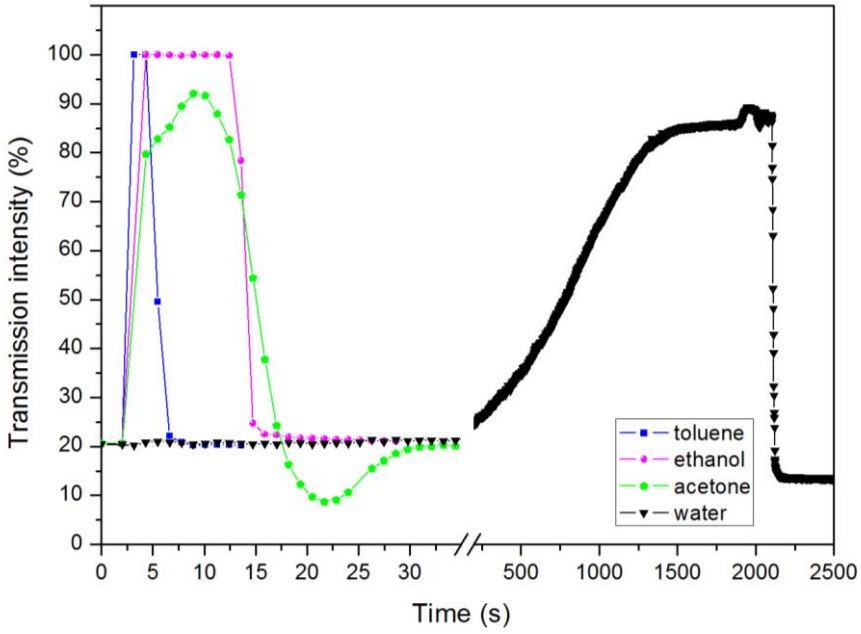

Figure 3.12 - Variation of the light transmission intensity of the dry 60PU/40PBDO UV-irradiated elastomeric film during the sensing response to the dripping of a different solvent, toluene, ethanol, acetone and water, droplet at the top of its surface.

Table 3.2 resumes the response of the elastomeric film sensor to the solvent dripped in its surface in terms of transmission intensity and response time. Basically the fastest response was obtained for the toluene with 1,1s: and the detection of ethanol was also fast 2,3s for the same transmission intensity (100% - transparent stage). The sensor spent 7s to detect the acetone and 26min for the water.

Table 3.2 - Transmission intensity and response time for several solvents dripped atop the surface of the 60PU/40PBDO prototype sensor.

Solvent	**Transmission intensity (%)**	**Response time (s)**
Toluene	100	1,1
Ethanol	100	2,3
Acetone	92	7,0
water	86	1582,0

3.7. Microlithography

The procedure made in the production of the VOCs sensor opened new ideas in getting elastomeric urethane/urea thin films written with logos and patterns with different sizes and dimensions, depending on the size of the mask used.

The lithographic method used in the production of the PU/PBDO sensor prototype was used in order to write and reveal logos and patterns in a small scale. In fact, it is possible to decrease the scale of the logo according to the wavelength of the wrinkled pattern (λ=1 μm). Figure 3.13 I. shows the SEM image obtained for the macrometer-sized pattern (letter width about 600μm) used to build the prototype sensor. In a reduced scale, Figure 3.13 II shows the micrometer-size pattern, which results from a 6 times size reduction of the impressed pattern on the mask. In this case, the letter width is about 100μm.

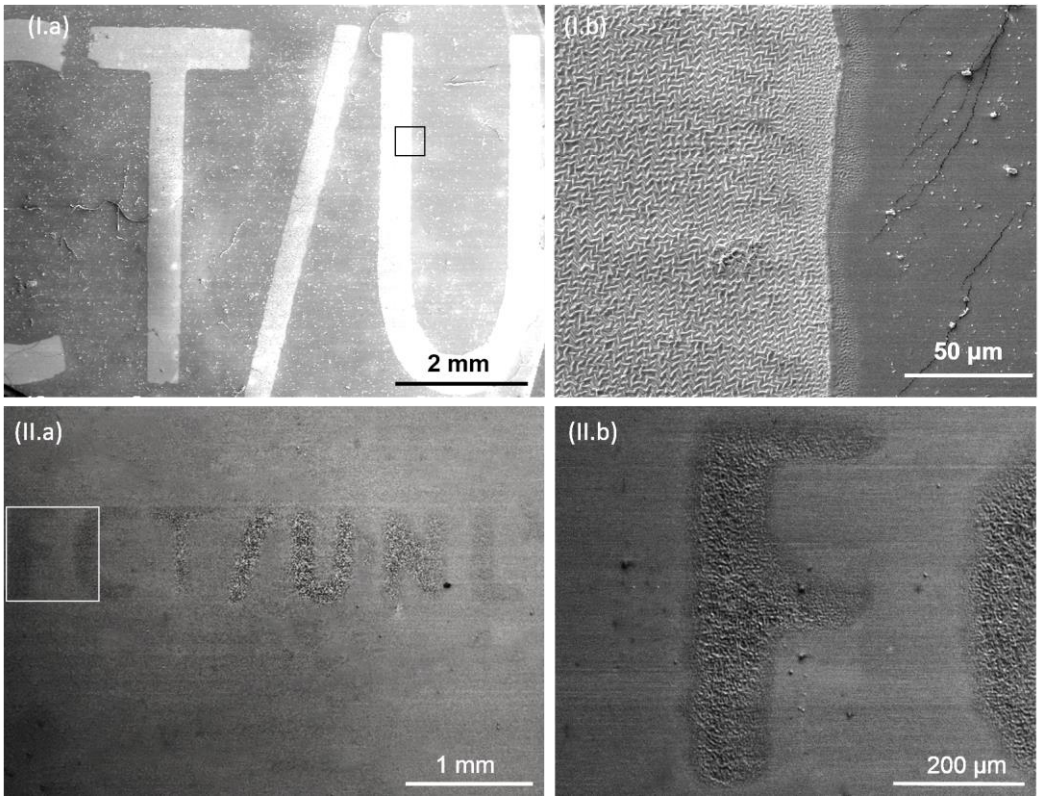

Figure 3.13 – SEM images: (I.a) macrometer-size pattern used for the VOCs sensor with a letter width about 600μm; (I.b) higher magnification image of the highlighted area represented in (I.a) shows the interface between the wrinkled and smooth surfaces; (II.a) micromter-size pattern obtained for a 6 times size reduction in comparison with the figure (I.a); (II.b) higher magnification image of the highlighted area represented in (II.b) herein the 'F' letter width is about 100μm.

Chapter 4 – Conclusions and Future Perspectives

In this work it is reported measurements of light scattering and microscopy imaging of poly(urethane-urea) free-standing films, irradiated for 24h with UV light (λ_{UV} =254nm) and extracted in toluene for several hours (varied from 3,5h to 27h). The data obtained allowed to proceed in the understanding of fundamental and structure level of the wrinkled PU/PBDO system behavior: wavelength and amplitude of the wrinkles. In previous work the wrinkle features that appeared in this kind of elastomeric spheres, amplitude and wavelength, were investigated by varying essentially the particle diameter and swelling conditions. In this work, it is reported that the membrane surface can develop diverse wrinkled patterns, depending on the time of solvent extraction in the *Soxhlet* apparatus. It was found that the development of micrometer features at the surface of the elastomeric membrane is primarily driven by UV radiation exposure (*i.e.*, it is the time of exposition to the UV light that determines the wavelength of the wrinkles in the surface), while the variation of the amplitude of the wrinkled surface is mainly related to the *sol* extraction during *sol-gel* procedure (more time of extraction in toluene, more translucent is the final membrane).These observations seems to indicate that two different experimental methods are present in the PU/PBDO system, which are at the origin of the diverse 3D patterns that are possible to obtain at the surface of the membrane.

Some new ideas arisen from this work that should be undertaken. All the samples studied in this work were swollen up to their maximum swelling in toluene and, so, it was not possible to determine the experimental critical strain for what the wrinkles appeared. So, the detailed study of what is happening between 0h until 3,5h of extraction time should be performed. These data can be compared with the mathematical model proposed by equation 3, that relates the wrinkle amplitude to strain although the nature of the wrinkles in the PU/PBDO system is different from the one that gave rise to the model.

The understanding of fundamental behavior of the wrinkles (wavelength and amplitude) enabled the fabrication of a VOCs sensor from a PU/PBDO membrane. In this work is described a simple method to fabricate a sensor for VOCs from a single urethane/urea elastomeric membrane. Wrinkles were generated at the top of the membrane by selectively UV-irradiating part of the elastomeric free-standing film (photolithography process), followed by swelling and drying in toluene. This method of writing and revealing logos and patterns in the surface of these elastomeric thin films can be scaled above the tens of micrometer (until 1 μm, that is the wavelength of the wrinkles), with a much higher sensitivity than the common printers.

The preliminary data presented in this work afforded a new application for the urethane/urea elastomers: sensing VOC´s. Although the data presented are encouraging, this sensor needs to be tested for lower concentrations of solvents (namely liquid toluene diluted) and for gases sensing in a controlled saturated chamber.

Bibliography

[1] H.O. Jacobs, G.M. Whitesides, Submicrometer patterning of charge in thin-film electrets., Science. 291 (2001) 1763–6.

[2] M.J. Dalby, M.O. Riehle, S.J. Yarwood, C.D.. Wilkinson, A.S.. Curtis, Nucleus alignment and cell signaling in fibroblasts: response to a micro-grooved topography, Exp. Cell Res. 284 (2003) 272–280.

[3] B. Farshchian, S.M. Hurst, J. Lee, S. Park, 3D molding of hierarchical micro- and nanostructures, J. Micromechanics Microengineering. 21 (2011) 035016.

[4] G. Shi, N. Lu, H. Xu, Y. Wang, S. Shi, H. Li, et al., Fabrication of hierarchical structures by unconventional two-step imprinting., J. Colloid Interface Sci. 368 (2012) 655–9.

[5] L.J. Guo, Nanoimprint Lithography: Methods and Material Requirements, Adv. Mater. 19 (2007) 495–513.

[6] C. Acikgoz, M. a. Hempenius, J. Huskens, G.J. Vancso, Polymers in conventional and alternative lithography for the fabrication of nanostructures, Eur. Polym. J. 47 (2011) 2033–2052.

[7] O. Lyutakov, J. Tůma, I. Huttel, V. Prajzler, J. Siegel, V. Švorčík, Polymer surface patterning by laser scanning, Appl. Phys. B. 110 (2013) 539–549.

[8] J. Rodríguez-Hernández, Wrinkled interfaces: Taking advantage of surface instabilities to pattern polymer surfaces, Prog. Polym. Sci. (2014).

[9] M. Kryuchkov, V.L. Katanaev, G. a Enin, A. Sergeev, A. a Timchenko, I.N. Serdyuk, Analysis of micro- and nano-structures of the corneal surface of Drosophila and its mutants by atomic force microscopy and optical diffraction., PLoS One. 6 (2011) e22237.

[10] L. Mate, R.A. Hlavata, B. Meissner, Polybutadiene-Based Polyurethanes with Controlled Properties : Preparation and Characterization, Jounal Appl. Polym. Sci. 77 (2000) 381–389.

[11] S. Gogolewski, Selected topics in biomedical, Colloid Polym. Sci. 785 (1989) 757–785.

[12] J. Blackwell, K.H. Gardner, Structure of the hard segments in polyurethane elastomers, Polymer. 20 (1979) 13–17.

[13] M.H. Godinho, a C. Trindade, J.L. Figueirinhas, L. V Melo, P. Brogueira, a M. Deus, et al., Tuneable micro- and nano-periodic structures in a free-standing flexible urethane/urea elastomer film., Eur. Phys. J. E. Soft Matter. 21 (2006) 319–30.

[14] C. Zhao, M.N. De Pinho, Design of polypropylene oxide / polybutadiene bi-soft segment urethane / urea polymer for pervaporation membranes, Polymer. 40 (1999) 6089–6097.

[15] M.H. Godinho, a C. Trindade, J.L. Figueirinhas, L. V Melo, P. Brogueira, Study of micro and nano surface structures from UV irradiated urethane/urea elastomers., Biomol. Eng. 24 (2007) 97–101.

[16] J. Genzer, J. Groenewold, Soft matter with hard skin: From skin wrinkles to templating and material characterization, Soft Matter. 2 (2006) 310.

[17] K. Efimenko, M. Rackaitis, E. Manias, A. Vaziri, L. Mahadevan, J. Genzer, Nested self-similar wrinkling patterns in skins., Nat. Mater. 4 (2005) 293–7.

[18] M. Tokita, K. Miyamoto, T. Komai, Polymer network dynamics in shrinking patterns of gels, J. Chem. Phys. 113 (2000) 1647.

[19] T. Tanaka, Mechanical instability of gels at the phase transition, Lett. to Nat. 325 (1987) 786–789.

[20] H. Burrell, High Polymer Theory of the Wrinkles Phenomenon, Ind. Eng. Chem. Res. 46 (1954) 2233–2237.

[21] K. Huraux, T. Narita, B. Bresson, C. Frétigny, F. Lequeux, Wrinkling of a nanometric glassy skin/crust induced by drying in poly(vinyl alcohol) gels, Soft Matter. 8 (2012) 8075.

[22] R. Rizzieri, L. Mahadevan, a Vaziri, a Donald, Superficial wrinkles in stretched, drying gelatin films., Langmuir. 22 (2006) 3622–6.

[23] S.K. Basu, L.E. Scriven, L.F. Francis, a. V. McCormick, Mechanism of wrinkle formation in curing coatings, Prog. Org. Coatings. 53 (2005) 1–16.

[24] A.C. Trindade, M.H. Godinho, Pattern Formation in a bi-soft segment urethane elastomer, Mol. Cryst. Liq. Cryst. 412 (2004) 1703–1711.

[25] A.C. Trindade, M.H. Godinho, J.L. Figueirinhas, Shear induced finite orientational order in urethane/urea elastomers, Polymer. 45 (2004) 5551–5555.

[26] J.Y. Chung, A.J. Nolte, C.M. Stafford, Surface wrinkling: a versatile platform for measuring thin-film properties., Adv. Mater. 23 (2011) 349–68.

[27] C.-M. Chen, S. Yang, Wrinkling instabilities in polymer films and their applications, Polym. Int. 61 (2012) 1041–1047.

[28] A. Schweikart, N. Pazos-Pérez, R. a. Alvarez-Puebla, A. Fery, Controlling inter-nanoparticle coupling by wrinkle-assisted assembly, Soft Matter. 7 (2011) 4093.

[29] N. Pazos-Pérez, W. Ni, A. Schweikart, R. a. Alvarez-Puebla, A. Fery, L.M. Liz-Marzán, Highly uniform SERS substrates formed by wrinkle-confined drying of gold colloids, Chem. Sci. 1 (2010) 174.

[30] H. Wu, S. Kustra, E.M. Gates, C.J. Bettinger, Topographic substrates as strain relief features in stretchable organic thin film transistors, Org. Electron. 14 (2013) 1636–1642.

[31] H.S. Kim, A.J. Crosby, Solvent-responsive surface via wrinkling instability., Adv. Mater. 23 (2011) 4188–92.

[32] T. Ohzono, H. Monobe, R. Yamaguchi, Y. Shimizu, H. Yokoyama, Dynamics of surface memory effect in liquid crystal alignment on reconfigurable microwrinkles, Appl. Phys. Lett. 95 (2009) 014101.

[33] J. Choi, S. Pyo, K. Lee, H. Ko, J. Kim, Transparent and flexible toluene sensor with enhanced sensitivity using adsorption caralyst-funcionlized graphene, in: Int. Conf. On. Micro Electro Mech. Syst., 2014: pp. 512–515.

[34] T. Alizadeh, F. Rezaloo, Toluene chemiresistor sensor based on nano-porous toluene-imprinted polymer, Int. J. Environ. Anal. Chem. 93 (2013) 919–934.

[35] T. Zhong, W. Zhao, F. Jiang, X. Liang, Toluene sensor combining NASICON with ZnTiO3 electrode, Sensors Actuators B Chem. 202 (2014) 1103–1108.

[36] M. Partridge, R. Wong, S.W. James, F. Davis, S.P.J. Higson, R.P. Tatam, Long period grating based toluene sensor for use with water contamination, Sensors Actuators B Chem. 203 (2014) 621–625.

[37] L. Wang, S. Wang, M. Xu, X. Hu, H. Zhang, Y. Wang, et al., A Au-functionalized ZnO nanowire gas sensor for detection of benzene and toluene., Phys. Chem. Chem. Phys. 15 (2013) 17179–86.

[38] M.H. Godinho, a. C. Trindade, J.L. Figueirinhas, D. Vidal, L.V. Melo, P. Brogueira, Organized structures obtained from urethane/urea elastomers, Synth. Met. 147 (2004) 209–213.

[39] M.H. Godinho, a. C. Trindade, J.L. Figueirinhas, L. V. Melo, P. Brogueira, 3D Soft Microlithography in Segmented Anisotropic Urethane/Urea Elastomers, Mol. Cryst. Liq. Cryst. 437 (2005) 53/[1297]–61/[1305].